Available online at www.sciencedirect.com
SCIENCE DIRECT
Polymer 46 (2005) 7931–7944
polymer
www.elsevier.com/locate/polymer

Composite polymeric particles with ZnS shells

Andrij Pich[a,*], Jessica Hain[a], Yuri Prots[b], Hans-Juergen Adler[a]

[a]*Institute of Macromolecular Chemistry, Dresden University of Technology, Mommsenstr. 4, 01062 Dresden, Germany*
[b]*Max Planck Institute of Chemical Physics of Solid Materials, D-01187 Dresden, Germany*

Received 21 March 2005; received in revised form 13 May 2005; accepted 6 June 2005
Available online 20 July 2005

Abstract

We report on a preparation of hybrid particles with polymeric cores and ZnS shells. Two types of monodisperse sterically stabilized polystyrene particles with hydroxyl-terminated PEG chains (PS/PEGMA) or β-diketone groups (PS/AAEM) on the surface have been prepared and characterized. Formation of ZnS layer on the surface of submicron particles has been studied by SEM and EDX. Deposition of ZnS on the surface of PS/PEGMA particles is not uniform and leads to formation of 'raspberry' morphology with rough surface. It has been found that presence of β-diketone groups on the particle surface leads to formation of well-defined ZnS layers. It has been assumed that such effect is due to the complexation of Zn cations by β-diketone groups leading to nucleation and growth of ZnS crystals on the polymer particle surface. Polymeric particles were completely covered with ZnS if the loaded amount of inorganic material was higher then 40 wt%. The thickness of ZnS layer on the particle surface can be easily varied by changing the ZnS load (in present study maximal thickness of the ZnS shell was 70 nm). It has been found that increase of the ultrasound power leads to considerable increase of the ZnS deposition on the particle surface without strong changes of the particle morphology. Hybrid particles have been investigated with XRD technique and their optical properties were studied by UV-spectroscopy. The colloidal stability of obtained particles was studied by separation analyser. Sedimentation experiments indicate that colloidal stability of obtained composite particles depends strongly on loaded ZnS amount and pH value of the aqueous medium. It has been found that highest sedimentation velocities (or maximum of instability) were determined by ZnS loads, which provide complete coverage of the particle surface. Increase of the ZnS layer thickness led to better stability of hybrid particles in aqueous medium.

Keywords: Core-shell morphology; Composite particles; Colloidal stability

1. Introduction

Fabrication of novel inorganic–organic functional hybrid materials with tailored properties that depend on the combination of components employed in the reaction process received increased interest in last decade. Materials for specific applications in catalysis, electronics, biomaterials engineering can be designed by careful selection of the components and template morphology. Polymeric particles are attractive templates for deposition of inorganic materials due to their controlled dimensions, narrow particle size distribution, and controlled morphology.

Zinc sulphide (ZnS) is widely used in numerous technical systems such as paints [1], solar cells [2], IR-windows [3] etc. Formation of ZnS colloids with defined size can be achieved by precipitation and aggregation methods [4,5]. There is a large number of reports in the literature about synthesis and characterization of ZnS nanoparticles in aqueous medium [6–12]. Preparation of composite materials on ZnS-basis can be divided into two parts, namely (a) composite materials with polymers and (b) well defined particles.

Huang et al. [13] reported synthesis of ZnS and $Zn_xCd_{1-x}S$ nano-composites in poly(methyl methacrylate-*co*-methacrylic acid) matrixes. By control of the monomer amount in copolymerization, different Zn/Cd ratio samples were obtained. It has been reported that the band gap energies of the nano-composites increased with increasing Zn content and different luminescence colours of the samples were obtained by adjusting the molar ratio between Zn and Cd.

* Corresponding author.
E-mail address: andrij.pich@chemie.tu-dresden.de (A. Pich).

0032-3861/$ - see front matter © 2005 Elsevier Ltd. All rights reserved.
doi:10.1016/j.polymer.2005.06.062

Ma et al. [14] reported preparation of hollow particles (50–70 nm) by synthesis of ZnS in aqueous solution in presence of triblock copolymer (Pluronic).

Polymeric particles containing ZnS have been prepared by utilizing microgel [15], SiO_2 [16] or polystyrene [17] particles as templates. Bai et al. [15] reported synthesis of composite microspheres containing ZnS with patterned structures by using poly(*N*-isopropylacrylamide-*co*-methacrylic acid) microgels as templates. It has been reported that the surface structures of obtained particles depends strongly on the ratio of the metal sulphide to the template, indicating that microgel network plays role of confinement and guidance of the precipitation of ZnS. Velikov et al. [16] used silica particles for deposition of ZnS or vice versa for preparation of core-shell structures. Formation of well-defined ZnS layers on SiO_2 surface was achieved and hollow particles were obtained after removal of silica core. Deposition of ZnS on the surface of polystyrene particles modified with carboxylic groups has been reported by Breen et al. [17]. The ZnS deposition process on the particle surface leads to formation of 70–80 nm thick uniform zinc sulphide layers.

In present paper, we report preparation of ZnS shells on the surface of polystyrene particles bearing hydroxyl-terminated PEG chains on the surface or β-diketone groups. Our aim was to study the influence of the particle surface nature and deposited ZnS amount on the morphology of the formed inorganic layer. Additionally, performed stability investigations for obtained hybrid particles should give a better understanding of the stabilization mechanism in such complicated colloidal systems.

2. Experimental

2.1. Materials

Styrene (ST) (from Fluka) and acetoacetoxyethyl methacrylate (97%) (AAEM) (from Aldrich) were purified by conventional methods and then vacuum distilled under nitrogen. ω-Hydroxy poly(ethylene glycol)methacrylate (PEGMA, Aldrich) with average $M_w = 526$ g/mol was used as supplied. Sodium peroxydisulfate (97%) (SPDS), zinc acetate ($Zn(Ac)_2$), thioacetamide (TAA) were received from Aldrich and used as commercially available. Distilled water was employed as polymerization medium.

2.2. Synthesis of PS/AAEM core particles [18]

Double-wall glass reactor equipped with stirrer and reflux condenser was purged with nitrogen. Water (170 g) and appropriate amount of ST (19.5 g) and AAEM (0.5 g, 2.5% to ST) were added into reactor and stirred at room temperature. After 10 min temperature was increased to 70 °C and water solution of initiator SPDS (0.3 g in 10 g water) was added to start the polymerization process. Latex was prepared at ca. 10% solid content.

2.3. Synthesis of PS/PEGMA core particles [19]

Double-wall glass reactor equipped with stirrer and reflux condenser was purged with nitrogen. Water (170 g) and appropriate amount of ST (19.5 g) and PEGMA (0.5 g, 2.5% to ST) were added into reactor and stirred at room temperature. After 10 min temperature was increased to 70 °C and water solution of initiator (0.3 g in 10 g water) was added to start the polymerization process. Latex was prepared at ca. 10% solid content.

2.4. Synthesis of composite particles

Preparation of ZnS-containing composite particles has been performed by method described by Breen et al. [17]. Diluted PS/AAEM dispersions were placed into glass vessel, $Zn(Ac)_2$ and TAA solution was added ($Zn(Ac)_2$:TTA molar ratio was 1:1). Reaction mixture was ultrasonically agitated by titanium tip immersed directly into the solution (Branson Sonifier, power output 90 W, pulsed operation regime 20%). After 6 h formed composite particles were removed from reaction vessel and cleaned by precipitation to remove all by-products. The pH of purified dispersions was around 5.8.

2.5. Analytical methods

A commercial laser light scattering (LLS) spectrometer (ALV/DLS/SLS-5000) equipped with an ALV-5000/EPP multiple digital time correlator and laser goniometer system ALV/CGS-8F S/N 025 was used with a helium–neon laser (Uniphase 1145P, output power of 22 mW and wavelength of 632.8 nm) as the light source. In dynamic LLS the Laplace inversion (the CONTIN procedure) of each measured intensity–intensity–time correlation function $G^{(2)}(q,t)$ in the self-beating mode can be related to a line-width distribution $G(\Gamma)$. For a pure diffusive relaxation, Γ is related to the translational diffusion coefficient D by $\Gamma/q^2 = D$ at $q \to 0$ and $c \to 0$, or a hydrodynamic radius R_h by $R_h = k_B T/(6\pi\eta D)$ with k_B, T and η being the Boltzmann constant, absolute temperature, and solvent viscosity, respectively. Accuracy of measurements for hydrodynamic radius $\pm 3\%$.

For careful determination of the particle size distribution samples were characterized with flow-field-flow-fractionation coupled with multi-angle-laser-light-scattering (F-FFF-MALLS). The fractionator F-100 (FFFractionation, Inc., Salt Lake City, USA) and DAWN-DSP light scattering photometer (Wyatt Technology Corp., Santa Barbara, USA) were used. Obtained data were interpreted by using ASTRA 4.50 software from Wyatt Technology Corp. Solvent for F-FFF-MALLS measurements was deionized water containing 0.02% (w/w) SDS and 0.02% (w/w) NaN_3 as a bactericide. Samples were measured at constant cross flow

rates. Scattering intensities are monitored continuously using a MALLS photometer with up to 18 detectors at fixed angles between 10 and 160°. Values for the molar mass M_w and radius of gyration $\langle R_g^2 \rangle_z^{0.5}$ at each 'slice' along the elution process can be calculated using the following equations:

$$\frac{Kc}{R_\theta} = \frac{1}{M_w P(\theta)} + 2A_2 c + \ldots \quad (1)$$

$$P(\theta) = 1 - \frac{1}{3}\left(\frac{4\pi n_0}{\lambda_0}\right)^2 \langle R_g^2 \rangle_2 \sin^2\left(\frac{\theta}{2}\right) \quad (2)$$

where K is a light scattering constant, containing the wavelength λ_0 of the incident light, a refractive index n_0 of the pure eluent, and the refractive index increment dn/dc; c is a sample concentration; A_2 is the second virial coefficient; R_θ is the excess Rayleigh ratio and $P(\theta)$ is a scattering function. For very diluted solutions, the second and higher order terms in Eq. (1) can be neglected and R_θ becomes directly proportional to $M_w P(\theta)$. Plotting R_θ/Kc against $\sin^2(\theta/2)$ gives M_w from the intercept with the ordinate and $\langle R_g^2 \rangle_z^{0.5}$ from the angular dependence of the intensity of the scattered light. This method is referred to as Debye-method and is more suitable for large particles, which show more curved scattering function (Mie-scattering). Calculations were made with polynomial fit of different orders between 1 and 3 in order to describe the scattering curve.

Scanning electron microscopy (SEM) images were taken with Gemini microscope (Zeiss, Germany). Samples were prepared in the following manner. Dispersions were diluted with deionized water, dropped onto aluminium support and dried at room temperature. Samples were coated with thin Au/Pd layer to increase the contrast and quality of the images. Pictures were taken at voltage of 4 kV.

Energy-dispersive X-ray analysis (EDX) has been carried out with X-ray analyser coupled with SEM Gemini microscope (Zeiss, Germany).

Thermo gravimetrical analysis (TGA) (TGA 7, Perkin–Elmer) was used to determine the ZnS content in composite particles. Before measurement samples were dried in vacuum for ca. 48 h. Samples were analysed in open Al_2O_3 cups in temperature range 25–800 °C (heating rate 5 K/min in nitrogen atmosphere).

Stability measurements were performed with separation analyser LUMiFuge 114 (L.U.M. GmbH, Germany). Measurements were made in glass tubes at acceleration velocities from 500 to 3000 rpm. The slope of sedimentation curves was used to calculate the sedimentation velocity and to get information about stability of the samples.

UV spectra were recorded with Perkin–Elmer UV–vis spectrometer Lambda 45. This device was equipped by RSA-PE-20 accessory, which is an optical bench, including transfer optics, an integrating sphere and detector pre-amplification module. Samples were fixed between two quartz plates (layer thickness approximately 0.5 mm).

X-ray diffraction (XRD) spectra of the composite ZnS-containing particles were recorded with Siemens P5005 powder X-ray diffractometer equipped with a Cu Kα (wavelength 1.540 Å) radiation source using the Diffracplus software.

Electrophoretic mobility has been measured with Zetasizer 2000, Malwern Instruments. pH was adjusted by addition of 0.01 M NaOH or 0.001 M HCl. Average value of at least 10 measurements was adopted as electrophoretic mobility of particles at certain pH value. Measured data have been used to calculate ξ—potential of composite particles.

3. Results and discussion

3.1. Preparation of polymeric particles

3.1.1. PS/PEGMA system

PS/PEGMA particles have been prepared by surfactant-free polymerization of styrene in presence of poly(ethylene glycol) methacrylate (PEGMA) [19]. It was established that such particles consist of compact hydrophobic polystyrene-rich core and hydrophilic PEGMA-rich swollen shell. Obtained particles were characterized by narrow particle size distribution and particle dimensions can be varied by changing the PEGMA content in the reaction mixture. In present study, PS/PEGMA particles (5% PEGMA) with average hydrodynamic radius 175 nm have been used.

Fig. 1 shows the size distribution curves for PS/PEGMA particles prepared at different PEGMA concentrations and SEM image of PS/PEGMA sample used for deposition of ZnS. Results presented in Fig. 1 indicate that particles are quite monodisperse. It was suggested that presence of brush-like PEGMA layer on the particle surface proved by TEM measurements [19] can provide sufficient stabilization for ZnS domains during preparation of composite particles.

3.1.2. PS/AAEM system

PS/AAEM particles have been prepared by surfactant-free copolymerization of styrene and acetoacetoxyethyl methacrylate (AAEM) [18]. Due to the hydrophilic character of AAEM it can be predominantly located on the particle surface after copolymerization process with styrene. Therefore, PAAEM chains provide some electro-sterical stabilization to formed particles due to presence of brush-like layer on the particle surface bearing some carboxyl groups originating from hydrolysis of AAEM. Similar to PS/PEGMA system it is easy to control the particle size by changing the amount of AAEM in reaction system. In present study PS/AAEM particles (5% AAEM) with average hydrodynamic radius 275 nm have been used.

Fig. 2 shows the particle size distribution curves of PS/AAEM particles prepared at different AAEM contents and SEM image of the sample used for deposition of ZnS indicating the monodisperse nature of obtained particles.

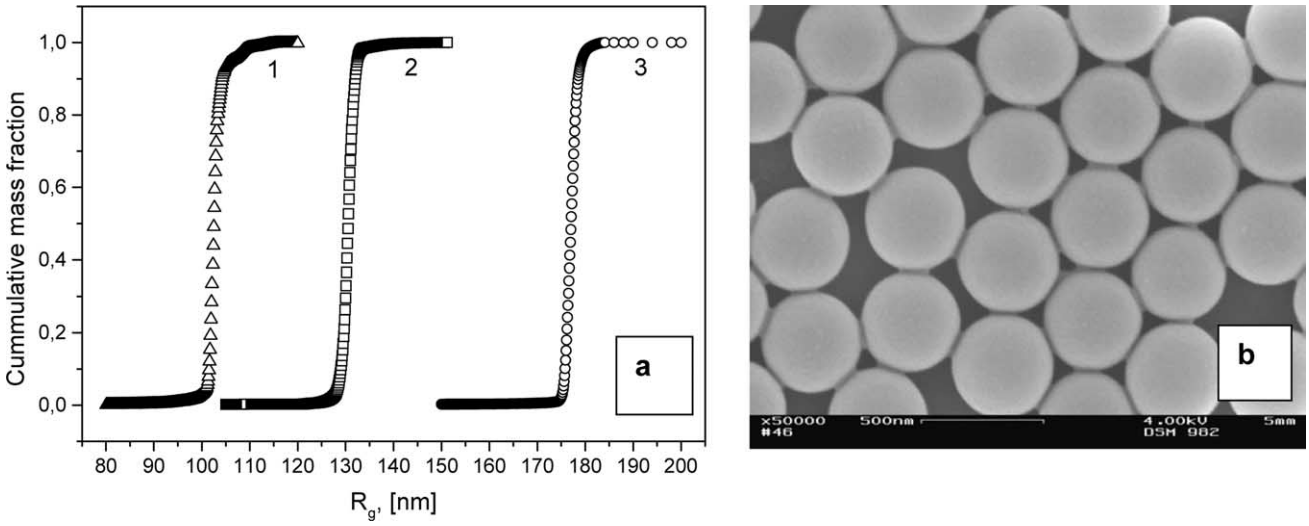

Fig. 1. Distribution curves of gyration radius (F-FFF data) of PS/PEGMA particles with different PEGMA contents: 1, 7.5; 2, 5; 3, 2.5% (a), and SEM image of PS/PEGMA particles with 5% PEGMA used in present study (b).

3.2. Deposition of ZnS

Ultrasonic method for preparation of ZnS has been frequently used by other research groups [20,21] and it seems that the mechanism of the ZnS formation in such conditions is more or less clear. In present research we focus mainly on the interaction of ZnS with the surface of the polymeric particles and we believe that the chemistry of zinc sulphide formation is not influenced by presence of polymeric particles. But reactive groups on the surface of the polymeric template can 'organize' the deposition process and the shell growth leading to more uniform coatings. Fig. 3(a) shows SEM image of ZnS prepared without polymeric particles. It is obvious that ZnS is present in form of separate particles with size from 50 to 150 nm. Closer look insight on these structures leads to conclusion that obtained particles consist of numerous ZnS nano-domains, which stick together.

The formation of such ZnS particles during sonification process can be explained by intensive agitation in the system and distribution of ZnS clusters on nano-scale. However, obtained particles are completely unstable and precipitate immediately when ultrasound is switched off.

The XRD pattern of ZnS shows the presence of three peaks (Fig. 3(d)), corresponding to the zinc blende crystal structure. Those diffraction peaks correspond to the (111), (220), and (311) planes of the cubic crystalline ZnS. This sample was prepared at similar conditions as hybrid particles but without polymeric beads in the system. The XRD pattern of hybrid particles shows also three weak broad peaks, which have similar position as pure ZnS. The presence of weak XRD signals in PS/AAEM/ZnS sample

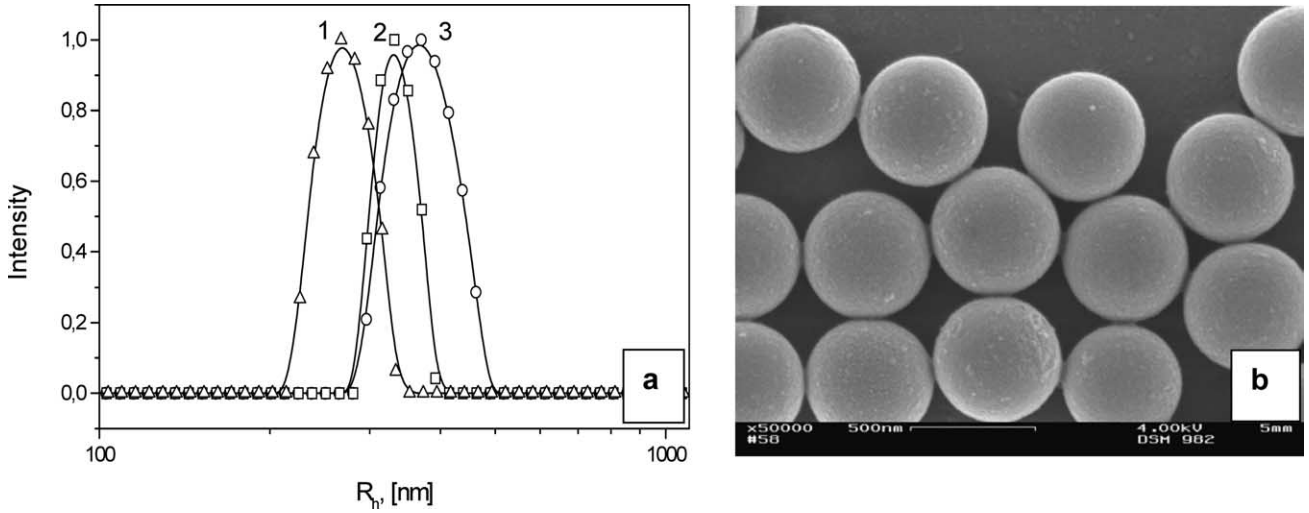

Fig. 2. Distribution curves of hydrodynamic radius (DLS data) of PS/AAEM particles with different AAEM contents: 1, 5; 2, 1.5; 3, 1% (a), and SEM image of PS/AAEM particles with 5% AAEM used in present study (b).

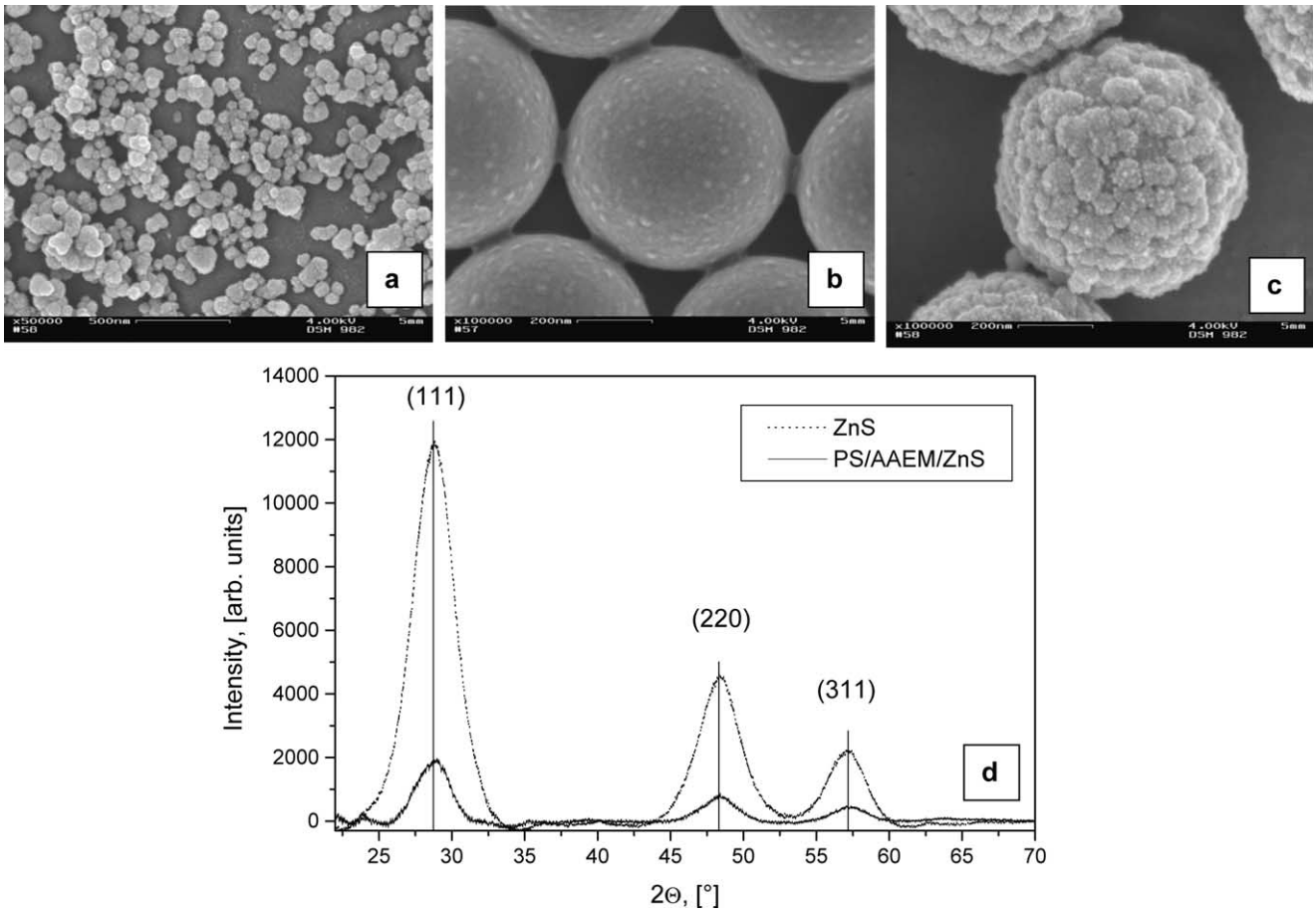

Fig. 3. SEM images of ZnS particles prepared without polymeric template (ingredients as for reaction 6 in Table 1 but without particles) (a), PS/AAEM core (b) and PS/AAEM/ZnS (32.55% ZnS) core-shell particles (c). X-ray powder diffraction spectrum of ZnS and PS/AAEM/ZnS particles (32.55% ZnS) (d).

can be attributed to the partial crystalline nature of ZnS and/or to the relatively small amount of ZnS (32.55%). SEM images in Fig. 3(b) and (c) show PS/AAEM core and PS/AAEM/ZnS (32.55% ZnS) core-shell particles, respectively. Presence of ZnS domains on the surface of polymeric particles is clearly visible from this microscopy data. The ZnS deposition process on the surface of polymeric particles will be discussed in details in following chapters.

3.2.1. PS/PEGMA/ZnS system

Deposition of ZnS onto PS/PEGMA surface was performed in the way that ZnS load was increased step-wise to see the evolution of the shell formation. Table 1 shows the amounts of the reagents used for different reactions and final ZnS content determined by TGA measurements.

Table 1
Ingredients used for preparation of PS/PEGMA/ZnS particles

Sample	Particles, (g)	$Zn(Ac)_2$, (g)	TAA, (g)	ZnS^M, (%)
1	4.358	0.491	0.168	0.92
2	4.361	1.965	0.673	2.62
3	4.023	3.625	1.241	6.76
4	3.696	4.996	1.710	14.66
5	4.018	7.241	2.479	18.95
6	4.834	10.890	3.728	25.09

T=40 °C; US output 90 W; M=value measured by TGA.

Formation of ZnS layer on the PS/PEGMA surface can be visualized by SEM measurements. Fig. 4 shows micrographs of composite particles with different ZnS load.

SEM images in Fig. 4 indicate that ZnS deposits on the particle surface forming discrete domains (ca. 10 nm), which are non-uniformly distributed on the surface of PS/PEGMA particles. Increase of inorganic material load leads to step-wise growth of ZnS islands (up to 40 nm) and larger amounts of patches appear on the particle surface. Finally, between 19 and 25% ZnS content raspberry morphology is formed and PS/PEGMA particles are more or less coated with inorganic material. These observations suggest that PEGMA layer on the particle surface does not provide really good affinity to formed ZnS nano-clusters and this leads to such non-organized formation and high roughness of the shell.

Fig. 5 shows the average thickness of the ZnS layer as a function of the ZnS load measured by scanning electron microscopy. It is clear that the more or less compact shell in this case is formed after ZnS load is more the 15% and there is also rapid increase of the shell thickness for samples prepared at higher ZnS contents.

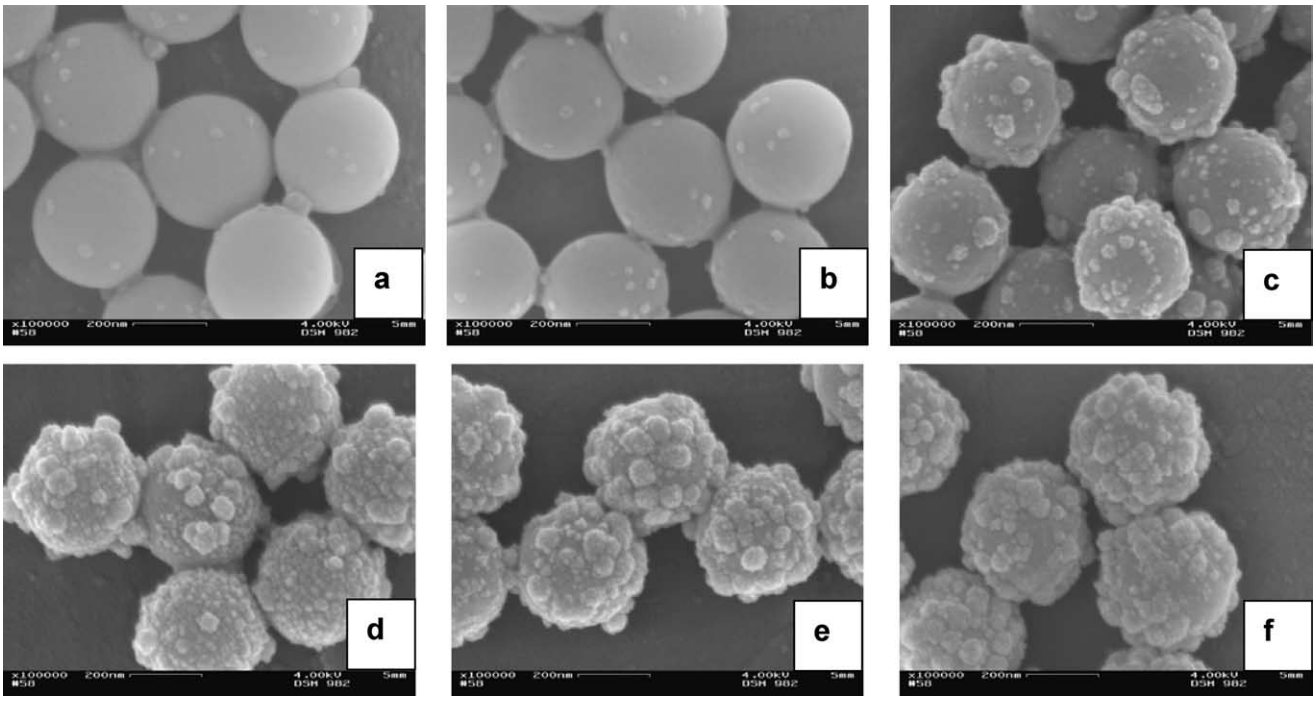

Fig. 4. SEM images of PS/PEGMA/ZnS particles prepared at different ZnS loads: (a) 0.92%; (b) 2.62%; (c) 6.67%; (d) 14.66%; (e) 18.95%; (f) 25.09%.

The kinetics of ZnS shell morphology formation on the polymer particle surface was followed by TGA and SEM measurements. In this case, samples were taken from reactor at certain time intervals and analysed by above-mentioned techniques. Fig. 6 shows results of thermogravimetrical analysis and it is clear that the ZnS content on the particle surface increases with sonication time. However, no linear increase of ZnS amount with time was observed in this case. Up to 80 min the ZnS content in the system was around 5% with next rapid increase to 20% within next 20 min. Later only very slow increase of ZnS amount in the system was determined and finally value of 25% has been reached.

Fig. 7 demonstrates SEM images of composite particles at different reaction times. The formation of ZnS coating visualized by microscopy is in good agreement with TGA measurements. The dramatic increase of ZnS content on the particle surface can be observed if one compares images (b) and (c) in Fig. 7.

At the present moment we do not have any reasonable explanation for such step-wise grows of ZnS domains on the PS/PEGMA surface. It can be suggested that in present system ZnS particles are generated predominantly in aqueous phase and probably after reaching certain size precipitate on the surface of polymeric particles. During nucleation in aqueous medium there is no considerable increase of ZnS in composite particles, since samples have

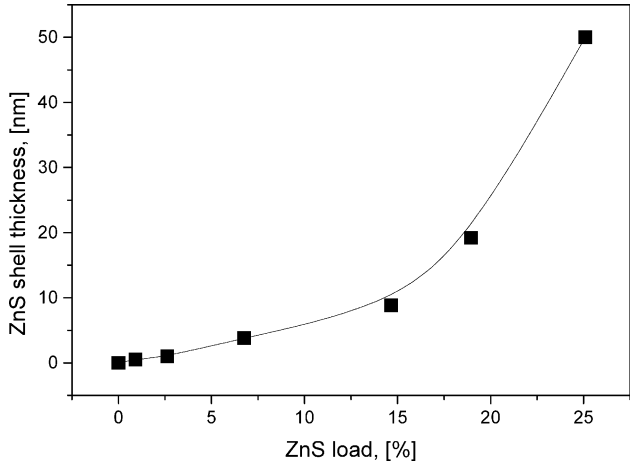

Fig. 5. Thickness of inorganic shell on the particle surface as a function of ZnS load.

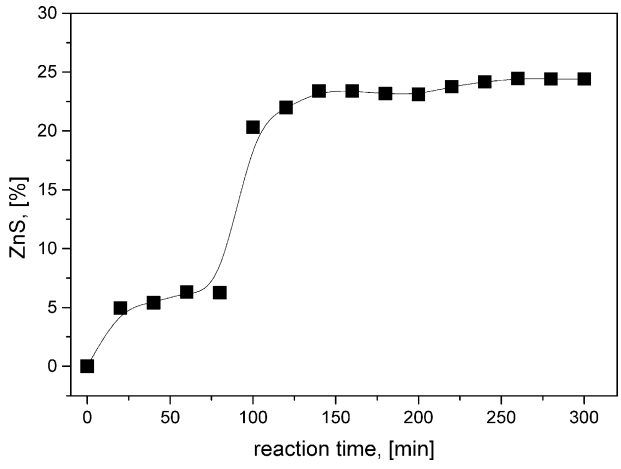

Fig. 6. Increase of ZnS amount on particle surface with reaction time (run 6 Table 1).

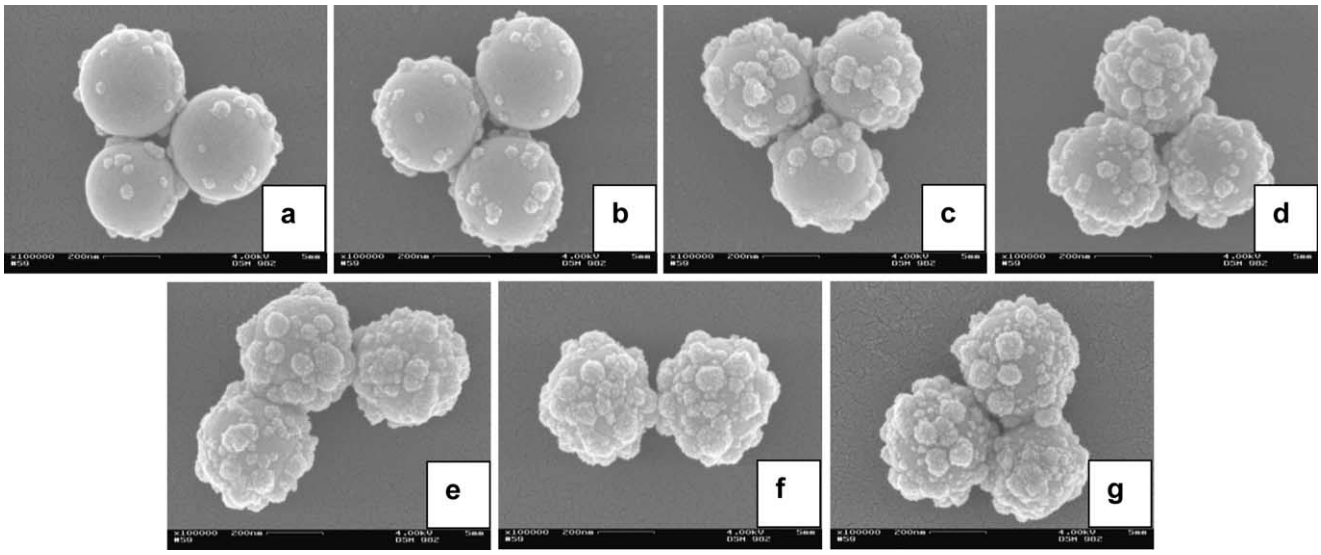

Fig. 7. SEM images of PS/PEGMA/ZnS particles (run 6) at different reaction times (min): (a) 20; (b) 60; (c) 120; (d) 180; (e) 240; (f) 300; (g) 360.

been cleaned prior to TGA measurements and all separate ZnS particles were removed. If to assume that coagulation of ZnS particles on the surface of polystyrene beads can be fast, so this can explain rapid increase of ZnS content observed in Fig. 6. It seems that in present system we observe two processes which occur simultaneously, namely appearance of new ZnS nano-domains on polymer particle surface and growth of ZnS nucleation centres in aqueous phase what leads finally to formation of composite beads by heterocoagulation and therefore rough particle surface and non-uniform inorganic coating.

3.2.2. PS/AAEM/ZnS system

Table 2 presents the amounts of reagents used for preparation of composite particles. Similarly to previous system the ZnS content was varied to obtain composite core-shell particles with different compositions.

Electron microscopy images of PS/AAEM/ZnS particles are presented in Fig. 8. One can see clearly that the particle morphology is different from PS/PEGMA/ZnS system. At low ZnS contents we observe similar effect—numerous small ZnS inclusions on the particle surface. But increase of ZnS content does not lead to growth of separate ZnS domains as observed earlier. Small zinc sulphide inclusions spread on the PS/AAEM particle surface and build up a dense layer approximately at 13% ZnS load and further increase of inorganic material content leads to uniform shell growth.

From these observations we can conclude that PS/AAEM particles are much more effective templates for ZnS deposition if to compare with PS/PEGMA spheres and provide controlled growth of ZnS shell. The reason for this effect is well known ability of β-diketone groups in AAEM structure to build complexes with different metals [22,23]. It can be assumed that this complexation of Zn ions provides their localization on the particle surface and further transformation to ZnS creates some nuclei for next intensive shell growth. After thermal decomposition of the polymer core hollow ZnS particles with highly porous shells can be obtained which depict clearly the morphology of the ZnS layer. The average thickness of the ZnS shell obtained from SEM measurements as a function of ZnS load is shown in Fig. 9. Results presented in Fig. 9 indicate that the shell thickness increases continuously and it is well-controlled by amount of loaded ZnS.

It is interesting to note that increase of the ultrasound power increases considerably the efficiency of the ZnS deposition on the PS/AAEM particle surface (Table 3).

It can be assumed that increase of the ultrasound power provides more quantitative reaction of TAA with $Zn(Ac)_2$ and therefore more complete formation of ZnS. SEM

Table 2
Ingredients used for preparation of PS/AAEM/ZnS particles

Sample	Particles, (g)	$Zn(Ac)_2$, (g)	TAA, (g)	ZnS^M, (%)
1	3.908	0.440	0.151	1.87
2	4.317	1.945	0.666	5.6
3	4.192	3.778	1.293	9.14
4	3.897	5.268	1.803	13.25
5	4.230	7.624	2.610	24.29
6	5.106	11.502	3.938	23.99
7	3.083	10.417	3.566	24.92
8	1.979	8.920	3.054	32.54

T=40 °C; US output 90 W; M=value measured by TGA.

Table 3
ZnS amount deposited at different ultrasound power

Sample	US, (W)	ZnS^M, (%)
1	90	23.99
2	270	41.26
3	360	42.49

M=value measured by TGA.

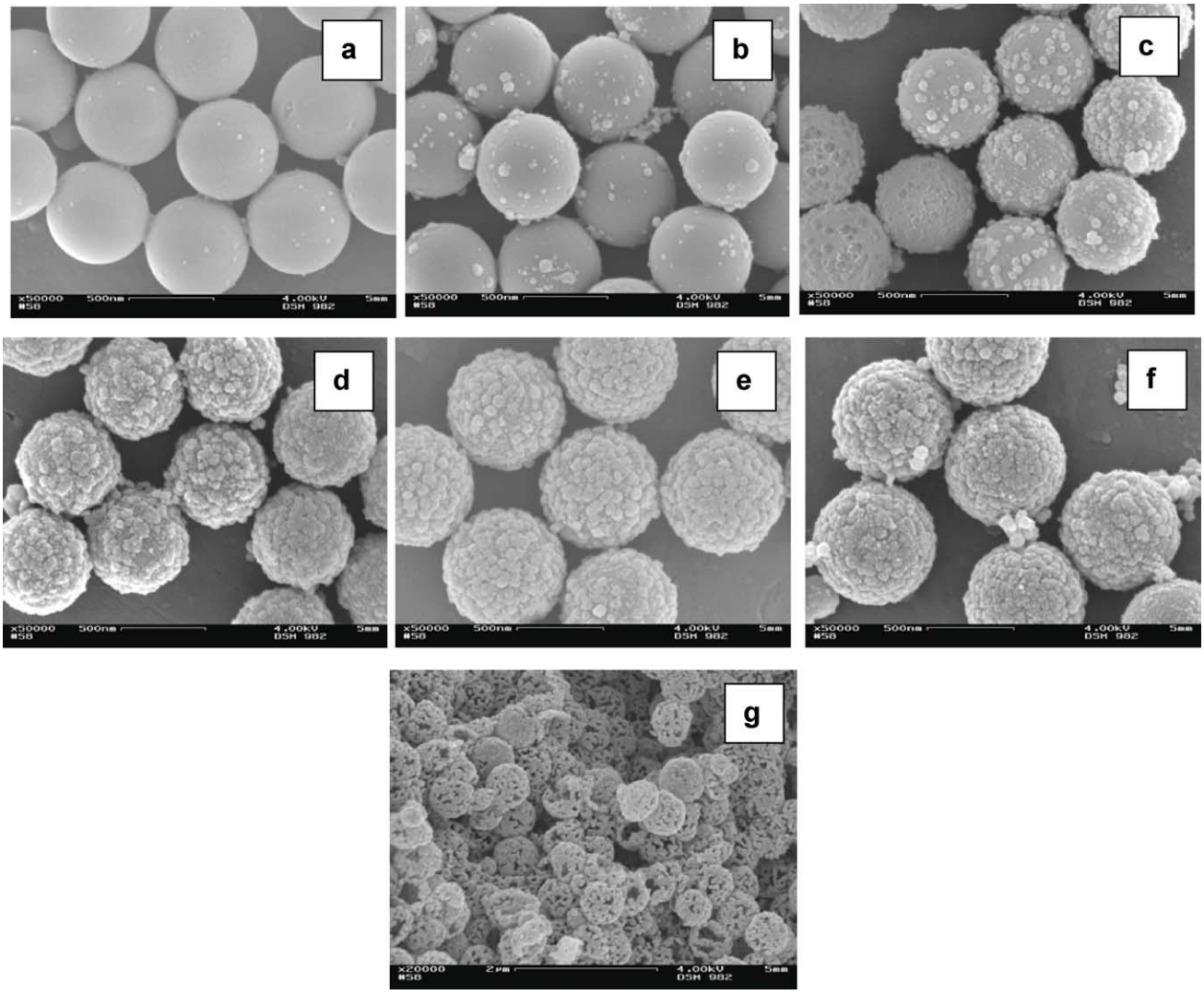

Fig. 8. SEM images of PS/AAEM/ZnS particles prepared at different ZnS loads: (a) 1.87%; (b) 5.6%; (c) 9.14%; (d) 13.25%; (e) 24.92%; (f) 32.55%. Image (g) shows mesoporous particles formed after thermal decomposition of PS/AAEM core of sample (e).

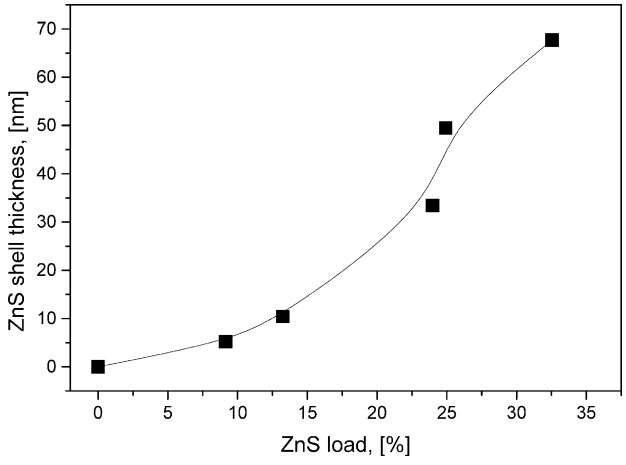

Fig. 9. Thickness of inorganic shell on the particle surface as a function of ZnS load.

images of obtained particles (not presented here) indicate that increase of the ultrasound power does not influence the morphology of the ZnS layer on the particle surface. Initially, low ultrasound power was selected for the preparation of composite particles because of possible degradation of the polymer chains and changes of the particle surface chemistry. But it seems that also variation of the ultrasound power is a powerful tool for control of the ZnS deposition process in the present system.

Similarly to PS/PEGMA system a kinetic measurement was performed at identical reaction conditions but PS/AAEM beads were used as templates. Results of kinetic measurement are presented in Fig. 10.

Fig. 10 indicates that in case of PS/AAEM system the evolution of ZnS amount with time proceeds in linear order. Similarly to PS/PEGMA system a rapid increase of ZnS content at initial stages of reaction is followed by slow increase of ZnS amount for more then 200 min. Comparing

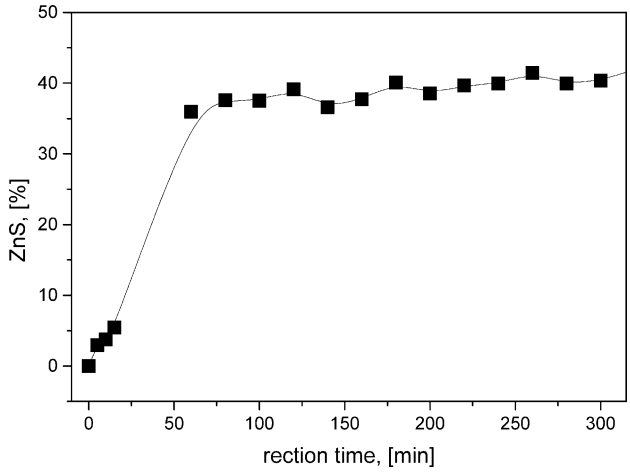

Fig. 10. Increase of ZnS amount on particle surface with reaction time (run 8 Table 1).

Fig. 6 and Fig. 10, one can clearly see that ZnS formation process is much faster in case of PS/AAEM system.

SEM images presented in Fig. 11 confirm clearly that formation of ZnS shell in present case is much faster comparing to PS/PEGMA system. After 20 min polymeric particles are nearly completely covered with ZnS. With increasing reaction time the ZnS shell becomes more compact and thicker what lead to some increase of the size of hybrid particles.

These observations prove that the surface of PS/AAEM particles has better affinity to ZnS what leads to accelerated appearance of ZnS nucleation zones and further formation of compact inorganic shell.

EDX analysis has been used for determination of the chemical structure of the particle surface. Fig. 12 shows a results of a complex EDX analysis performed for sample PS/AAEM/ZnS particles containing 23.99% ZnS. Fig. 12(a) shows the SEM image of the sample indicating the area used for EDX analysis. PS/AAEM/ZnS particles are randomly distributed on the Al support in one plane. Three particles forming a pearl-chain structure have been selected as a possible route for the line scan (a line shows the start and end point of the EDX line-scan).

Fig. 12(b) shows an EDX spectrum of the sample area investigated during line-scan indicating the strongest signals related to carbon and oxygen (from PS/AAEM core), Zn and S (from ZnS shell), and Al and Au (from support and contrast-enhancing coating, respectively). These data indicate clearly presence of ZnS on the particle surface. Additional element mapping has been performed on the same area (Fig. 12(c)). Intensity of the signal is proportional to the quantity of the certain element on selected area (see line in Fig. 12(a)). Bottom picture in Fig. 12(c) shows a

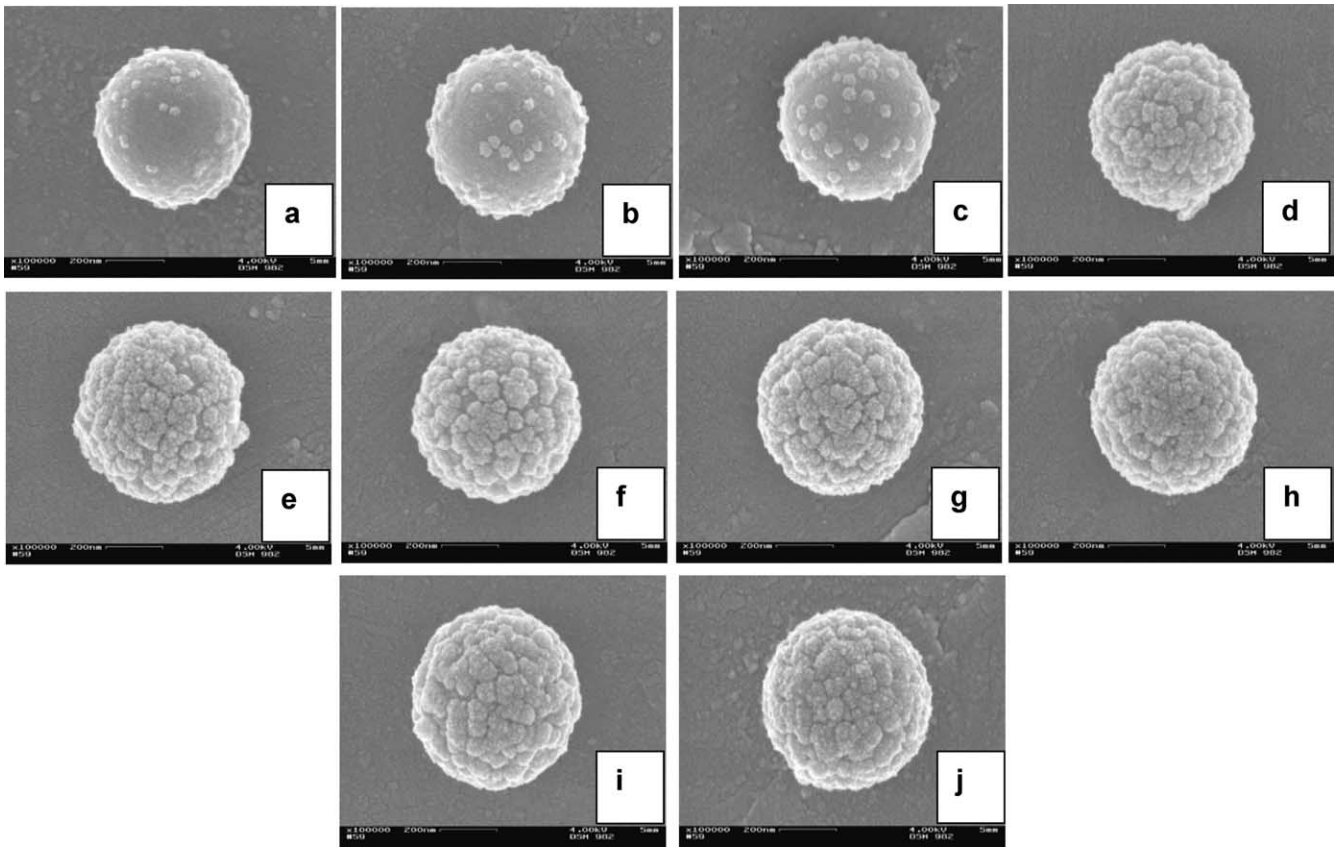

Fig. 11. SEM images of PS/AAEM/ZnS particles (run 6) at different reaction times (min): (a) 5; (b) 10; (c) 15; (d) 20; (e) 60; (f) 120; (g) 180; (h) 240; (i) 300; (j) 360.

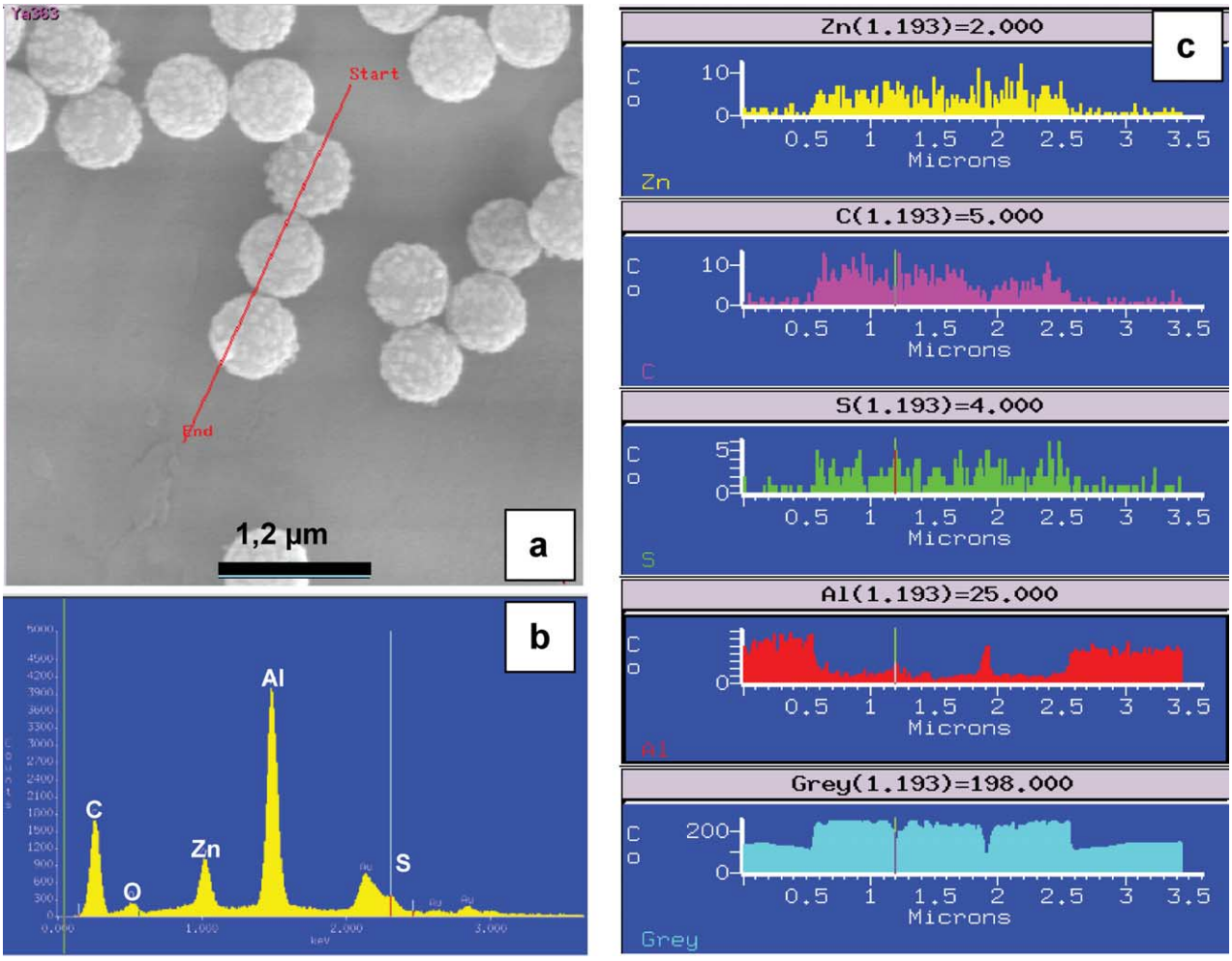

Fig. 12. SEM image of PS/AAEM/ZnS particles containing 23.99% ZnS indicating the area selected for EDX analysis (line shows the pathway of the line scan) (a); corresponding EDX spectrum (b); and element mapping along the line scan (c).

profile of the scan indicating clearly 3 PS/AAEM/ZnS particles selected for analysis. Fig. 12(c) indicates clearly that Zn and S are present only on the particle surface and very low signal intensity was detected beside composite spheres.

3.3. Particle characterization

3.3.1. Optical properties

UV/vis-measurements have been performed to characterize the optical properties of the composite core-shell particles. As shown in Fig. 13, sample prepared at smallest ZnS content showed an onset of absorption at ca. 350 nm. Increase of the ZnS content in the samples leads to the gradual shift of the onset absorption to higher wavelength. It is known that the UV/vis onset absorption of semiconductor particles is attributed to the band gap absorption and, as expected it should be red-shifted if ZnS particles grow in size. Similar effect was reported by Du et al. [24] for polystyrene particles with CdS shells.

3.3.2. Colloidal stability

The stability of polymeric beads and corresponding hybrid particles was investigated by sedimentation method developed by Lerche et al. [25]. In special centrifuge an integrated optoelectronic sensor system allows spatial and temporal changes of light transmission during the rotation to be detected. In contrast to other approaches [26], the local transmission is determined over the entire sample length simultaneously. Throughout the measurement, transmission profiles are recorded and sedimentation process can be depicted as a time course of the relative position of the boundary between supernatant and sediment (resolution better than 100 µm) or of the transmission averaged over the entire or a chosen part of the sample length. On the basis of obtained data the sedimentation constants, the packing density, etc. can be derived.

It has been found that original polystyrene dispersions were quite stable, but after deposition of ZnS some particle aggregation takes place. According to sedimentation studies, PS/AAEM particles precipitate faster than PS/PEGMA beads. Since in both cases particles are

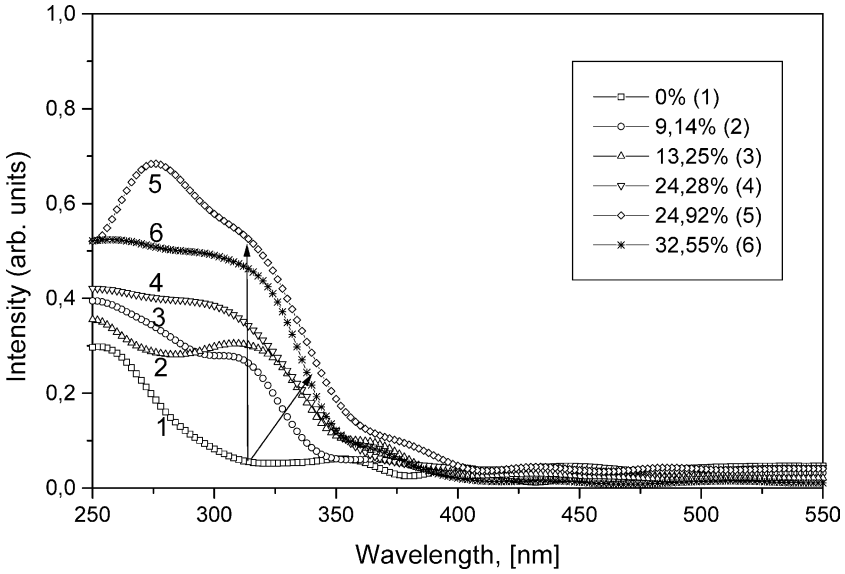

Fig. 13. UV–vis spectra of PS/AAEM/ZnS particles with different ZnS contents.

stabilized by sterical mechanism, the reason for such behaviour is the larger size of PS/AAEM particles. Better stability of PS/PEGMA particles can be additionally explained by presence of grafted poly(ethylene glycol) chains on the particle surface which prevent aggregation in aqueous solution [19].

Fig. 14 shows sedimentation velocity of PS/PEGMA/ZnS composite particles prepared at different ZnS contents calculated from the slope of the transmission–time curves.

For composite particles initially sedimentation velocity increases with ZnS load, reaches the maximum, and later decreases rapidly reaching the value close to the uncleaned samples. The initial increase of the sedimentation velocity can be explained by destabilization of particles due to the coverage of water-soluble PEGMA chains by ZnS domains and therefore lost of efficient steric stabilization. The improved stability of composite particles with ZnS load higher then 15% is difficult to explain. As it was mentioned before, for composites containing more then 15% ZnS inorganic shell covers the surface PS/PEGMA particles. It can be assumed that ZnS brings some electrostatic stabilization to composite particles, and this effect will be discussed more in details later together with measurements of electrophoretic mobility. Stability measurements presented in Fig. 14 indicate that generally PS/AAEM/ZnS particles are much more stable as their PS/PEGMA/ZnS analogues. Similarly to previous system, we observed an increase of sedimentation velocity with ZnS content and

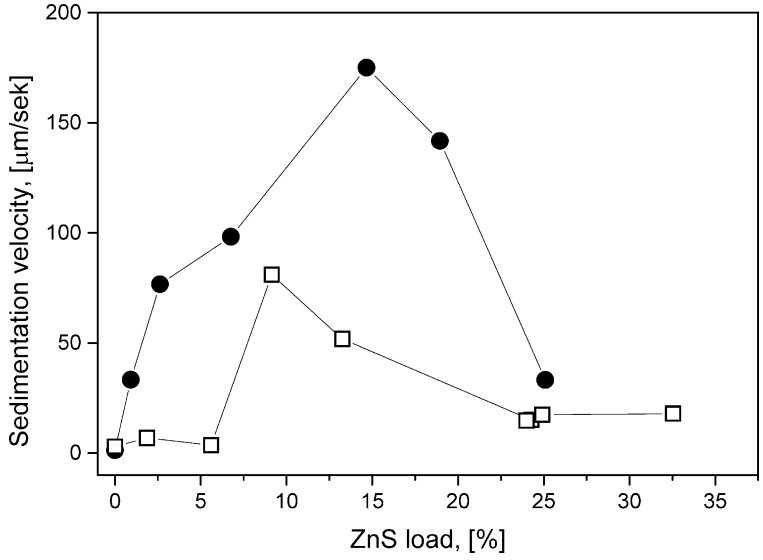

Fig. 14. Sedimentation velocity of PS/PEGMA/ZnS (solid symbols) and PS/AAEM/ZnS (open symbols) particles prepared at different ZnS loads (rotation speed—2000 rpm).

later gradual decrease. It is interesting to note, that in present case the sedimentation velocity decreases if the particle surface is completely coated with ZnS (similarly to PS/PEGMA/ZnS particles). Sedimentation measurements lead to conclusion that the stabilization mechanism of composite particles with ZnS layer on the surface can be probably explained by combination of some sterical stabilization provided by hydrophilic chains on the polymer particle surface and electrostatic stabilization by ionic groups of inorganic component.

3.3.3. Electrophoretic mobility

ξ-Potential measurements of selected samples are shown in Fig. 15. PS/AAEM particles and two PS/AAEM/ZnS samples with 9.14 and 32.55% ZnS on the surface have been investigated. According to Fig. 14, PS/AAEM/ZnS sample with 9.14% ZnS exhibits the highest sedimentation velocity (or lowest stability) if to compare with PS/AAEM core and PS/AAEM/ZnS sample with 32.55% ZnS.

Fig. 15 indicates clearly that PS/AAEM particles remain negatively charged in acidic and basic pH. Contrary, ZnS is positively charged in acidic medium and according to Ref. [27] possess isoelectrical point at pH = 5.5 (in our case measurements at pH < 5.5 were hindered due to very fast precipitation of ZnS). Following this, incorporation of ZnS on the PS/AAEM particle surface will lead to dramatic charge changes on the surface of composite spheres. Composite PS/AAEM/ZnS particles exhibit isoelectric point (see arrows in Fig. 15) and are positively charged at acidic pH what confirms deposition of the ZnS. Composite particles possess stronger positive charge in acidic medium if ZnS load increases. It should be noted that the pH value of PS/AAEM/ZnS particles after purification procedure was around 5.8. It is clear from Fig. 15 that PS/AAEM/ZnS particles containing 9.14% of inorganic material are nearly neutral in pH range 5.5–6, so this is the reason for the very high sedimentation velocity values reported in Fig. 14. If ZnS load is smaller then 9% composite particles should be negatively charged at this pH, because the charge of PS/AAEM particles will dominate. If ZnS load is very high the positive charge of ZnS shell, which covers completely the surface of polymeric spheres will protect particles from flocculation and precipitation. Therefore, the peak maxima observed in Fig. 14 for PS/PEGMA/ZnS and PS/AAEM/ZnS particles can be explained by minimal charge of the composite particles, which is present at the nearly complete coverage of the polymeric core with inorganic material. If the coverage with ZnS is incomplete—the electro-sterical stabilization provided by polymeric particles dominates. In case if the ZnS shell is build up, the positive charge will stabilize composite particles.

Additional experiment was performed to prove the reliability of the electrophoretic mobility measurements and stability tests. The sedimentation velocity of PS/AAEM/ZnS sample with 32.55% ZnS was measured at different pH values (similarly as *z*-potential measurement). Transmission–time curves obtained by analysing the experimental curves are shown in Fig. 16(a) indicating that beginning from pH = 7.2 the slope increases (particles precipitate faster) and calculated sedimentation velocity values increase rapidly (Fig. 16(b)).

These results correlate well with *z*-potential measurements shown in Fig. 15. In pH-range 7–8 PS/AAEM/ZnS particles with 32.55% ZnS on the surface exhibit isoelectrical point, so this is the reason for rapid increase of sedimentation velocity. It is unclear why the sedimentation velocity still increases in pH range from 8 to 10, since composite particles possess strong negative charge. Anyway, these data indicate that there is a good agreement between two experimental techniques and the combination of both gives a possibility to analyse more deeply different

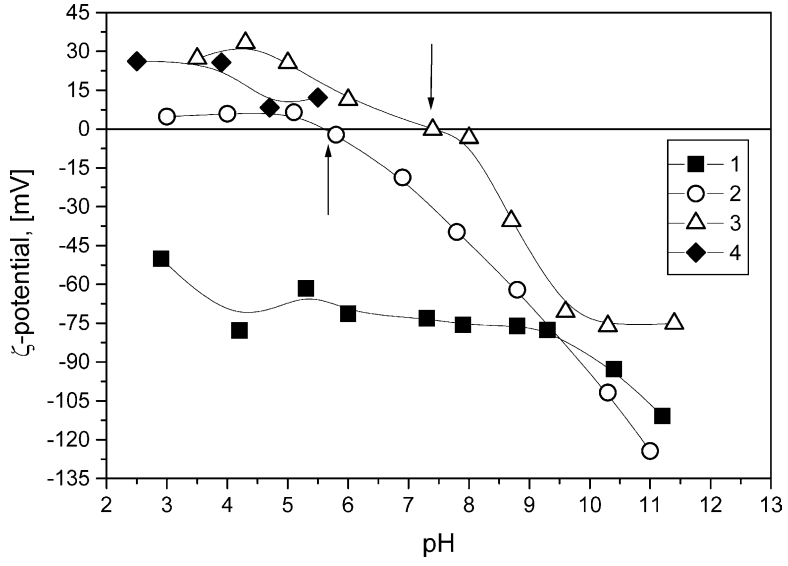

Fig. 15. ξ-Potential of particles as a function of pH: 1, PS/AAEM particles; 2, PS/AAEM/ZnS (9.14%); 3, PS/AAEM/ZnS (32.55%); and 4, ZnS particles.

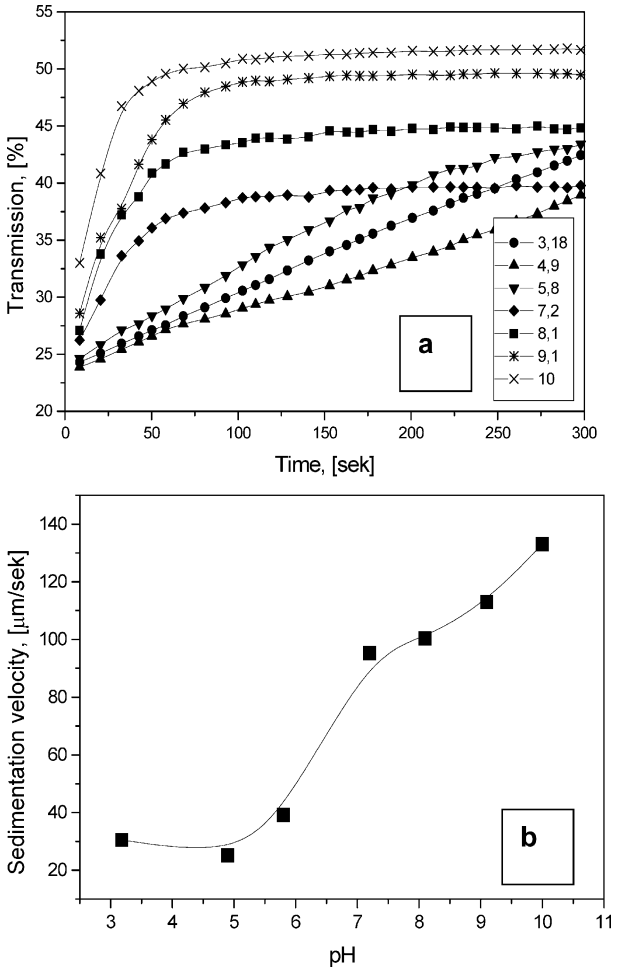

Fig. 16. Transmission–time curves (a) and calculated sedimentation velocity (b) for PS/AAEM/ZnS particles with 32.55% ZnS at different pH values.

phenomena related to stabilization of complex colloidal systems.

4. Conclusions

In present paper, we describe synthesis of hybrid particles with polymeric cores and ZnS shells. Two types of monodisperse sterically stabilized polystyrene particles with hydroxyl-terminated PEG chains (PS/PEGMA) or β-diketone groups (PS/AAEM) on the surface have been used as templates for deposition of the ZnS. Formation of ZnS layer on the surface of submicron particles has been studied by SEM and EDX. It has been found that deposition of ZnS on the surface of PS/PEGMA particles is not uniform and leads to formation of 'raspberry' morphology with rough surface. Contrary, presence of β-diketone groups on the particle surface leads to formation of more uniform ZnS layers. It has been assumed that such effect is due to the complexation of Zn cations by β-diketone groups leading to nucleation and growth of ZnS crystals on the polymer particle surface. Polymeric particles were completely covered with ZnS if the loaded amount of inorganic material was higher then 24.3 wt%. The thickness of ZnS layer on the particle surface can be easily varied by changing the ZnS load (in present study maximal thickness of the ZnS shell was 70 nm). It has been found that increase of the ultrasound power leads to considerable increase of the ZnS deposition on the particle surface without strong changes of the particle morphology. PS/PEGMA/ZnS and PS/AAEM/ZnS composite particles have been investigated with XRD technique and their optical properties were studied by UV-spectroscopy indicating typical properties of ZnS. The colloidal stability of obtained particles was carefully studied by separation analyser and measurements of electrophoretic mobility. Sedimentation experiments indicate that colloidal stability of obtained composite particles depends strongly on loaded ZnS. It has been found that highest sedimentation velocities (or maximum instability) were determined by ZnS loads, which provide complete coverage of the particle surface. Increase of the ZnS layer thickness led to better stability of hybrid particles in aqueous medium. Hybrid particles exhibit isoelectric point in pH range 6–8 and at this pH maximum of sedimentation velocity was detected indicating that the stability of such colloidal system depends strongly on the charge of the particle surface. Variable size of PS/AAEM and PS/PEGMA particles and flexible synthesis conditions of ZnS shell give a possibility to prepare composite particles with well-defined dimensions and controlled properties.

Acknowledgements

The authors are thankful to Mrs E. Kern for SEM measurements; Mrs I. Poitz for TGA investigations; Deutsche Forschungsgemeinschaft (DFG) with collaboration research project SFB 287 'Reactive Polymers' for financial support.

References

[1] Scholz SM, Vacassy R, Dutta J, Hofmann H, Akinc M. J Appl Phys 1998;83:7860.
[2] Yamaguchi T, Yamamoto Y, Tanaka T, Yoshida A. Thin Solid Films 1999;344:516.
[3] Harris DC. Infrared Phys Technol 1998;39:185.
[4] Wilhelmy DM, Matijevic E. J Chem Soc, Faraday Trans 1984;80:563.
[5] Williams R, Yocom PN, Sofko FS. J Colloid Interface Sci 1985;106:388.
[6] Rana RK, Zhang L, Yu JC, Mastai Y, Gedanken A. Langmuir 2003;19:5904.
[7] Xia B, Lenggoro W, Okuyama K. Chem Mater 2002;14:4969.
[8] Chen W, Joly AG, Malm J-O, Bovin J-O, Wang S. J Phys Chem B 2003;107:6544.
[9] Denzler D, Olschewski M, Sattler K. J Appl Phys 1998;84:2841.
[10] Scholz SM, Vacassy R, Dutta J, Hofmann H. J Appl Phys 1998;83:7860.

[11] Vogel W. Langmuir 2000;16:2032.
[12] Yanagida S, Ishimaru Y, Miyake I, Shiragami T, Pac C, Hashimoto K, et al. J Phys Chem 1989;93:2576.
[13] Huang J, Lianos P. Langmuir 1998;14:4342.
[14] Ma Y, Qi L, Ma J, Cheng H. Langmuir 2003;19:4040.
[15] Bai C, Fang Y, Zhang Y, Chen B. Langmuir 2004;20:263.
[16] Velikov KP, Blaaderen A. Langmuir 2001;17:4779.
[17] Breen ML, Dinsmore AD, Pink RH, Qadri SB, Ratna BR. Langmuir 2001;17:903.
[18] Pich A, Bhattacharya S, Adler HJ. Polymer 2005;46:1077.
[19] Pich A, Lu Y, Adler H-JP. Colloid Polym Sci 2003;281:907.
[20] Sostaric JZ, Caruzo-Hubson RA, Mulvaney P, Grieser F. J Chem Soc, Faraday Trans 1997;93:1791.
[21] Arul Dhas N, Zaban A, Gedanken A. Chem Mater 1999;11:806.
[22] Powell KR, McCleskey T, Tumas W, DeSimone JM. Ind Eng Chem Res 2001;40:1301.
[23] Schlaad H, Krasia T. Macromolecules 2001;34:7585.
[24] Du H, Xu Q, Chin WS. Chem Mater 2002;14:4473.
[25] Sobisch T, Lerche D. Colloid Polym Sci 2000;278:369.
[26] Killmann E, Eisenlauer J. Prog Colloid Polym Sci 1976;60:147.
[27] Wilhelmy DM, Matijevic E. J Chem Soc, Faraday Trans 1984;180:563.